Optics and Lasers in Engineering 48 (2010) 96–106

Contents lists available at ScienceDirect

Optics and Lasers in Engineering

journal homepage: www.elsevier.com/locate/optlaseng

Low-cost speckle interferometry for measuring 3D deformation fields: Hardware and software

Marco Bova, Luigi Bruno *, Andrea Poggialini

Department of Mechanical Engineering, University of Calabria, P. Bucci cubo 44C-87036 Arcavacata di Rende (CS), Italy

ARTICLE INFO

Article history:
Received 30 June 2009
Received in revised form
29 July 2009
Accepted 30 July 2009
Available online 26 August 2009

Keywords:
Speckle interferometry
Laser diode
Phase-shifting
Low-cost
3D deformation

ABSTRACT

In the present paper the authors propose a portable and low-cost speckle interferometer for evaluating 3D deformation fields. The interferometer was designed and realized with the aim of carrying out measurements on small areas, hence it can be used to approach problems characterized by displacement field with highly localized gradients, such as the strain relief occurring in residual stress evaluation or the displacements which arise around notches or crack tips. The costs of the experimental equipment were reduced by employing laser diodes as light sources, a PZT actuator designed and calibrated by the authors and a control electronics realized on purpose. Moreover the configuration which was adopted allows further saving on optical components. The experimental results reported at the end of the paper, and obtained by a specimen subjected to 3D rigid body motions, show a high repeatability and accuracy. Furthermore the experimental results have shown that the geometry of the optical setup implies the variation of the sensitivity vectors on the inspected area, but this effect can be evaluated (analytically and/or experimentally) and taken into account in order to increase the accuracy of the measurements.

1. Introduction

Speckle interferometric techniques, assessed in the late 1960s and the first 1970s, are nowadays powerful means for carrying out non-contact full-field measurements with high accuracy [1–3].

At the beginning this new family of interferometric techniques represented the natural evolution of the holographic techniques [4,5], basically due to their capability to be implemented without the expensive and time-consuming chemical processing of the holographic plates. However speckle techniques were still suitable for laboratory experiment only, due to the high cost of many equipments (i.e. coherent light sources, optical sensors, optical components) and the high sensitivity to the environmental background (i.e. mechanical vibrations, thermal gradients). Furthermore in the succeeding years the introduction of the phase-shifting procedures [6] introduced new expensive components (e.g. piezoelectric actuator).

Over the years, after speckle interferometry had become a well-assessed experimental technique [7–11], many researchers focused their efforts in order to obtain cheaper and lightweight devices, able to work properly also far from the anti-seismic bench and out of the controlled environment of the laboratory.

The parts whose weight and cost were strongly reduced over the years are the light sources and the piezoelectric actuators.

The most popular high coherence light sources for interferometric applications, after the laser invention in the 1960 [12], are based mainly on He–Ne and Ar-Ion technology. The first type is normally characterized by a low output power (<50 mW), while the second type by a very high power absorption (several kW) which normally requires proper cooling systems.

In the last years new types of light sources are diffusing for scientific applications, the laser diodes and the diode-pumped solid-state lasers. The laser diodes (Hitachi, Sanyo, Mitsubishi and Sharp are the major manufacturers) are very compact devices and normally available on the market in two geometrical versions, 5.6 and 9.0 mm packages. The single mode output power spans from few mW to 1 W and the wavelength from 400 to 1500 nm. In order to work properly the diode must be assembled into specific mounts and supplied with DC voltage controllers. These sources are very cheap, small and lightweight. Their drawbacks reside in the power and wavelength stability and in the mechanical weakness of the package.

The diode-pumped solid-state lasers – DPSSL – (Coherent is a well-known manufacturer) are more expensive sources than the laser diodes, but these are capable of providing high optical and mechanical stability, and a very high temporal coherence. Moreover a very high output power can be attained (up to 20 W) against a reduced input absorption if compared with the Ar-Ion lasers, and many portable versions are available too.

* Corresponding author.
E-mail addresses: marco.bova@unical.it (M. Bova), bruno@unical.it (L. Bruno), poggialini@unical.it (A. Poggialini).

0143-8166/$ - see front matter © 2009 Elsevier Ltd. All rights reserved.
doi:10.1016/j.optlaseng.2009.07.018

The piezoelectric actuators are one of the most popular types of phase-shifter used for interferometric applications. The most important limitation for these devices is not the weight or the size, but the cost; in fact, in order to ensure a very accurate control of the optical paths and due to the presence of non-linearity and hysteretic behavior, they are equipped with motion sensors and complex feedback control electronics, which obviously increase significantly the prices.

With the aim of disposing of a low-cost phase-shifter the researchers can follow essentially two approaches: adopting innovative hardware (mechanical and/or electrical) solutions [13,14], or implementing more or less complex software procedures able to predict accurately the electro-mechanical behavior of the actuator [15–17]. The literature regarding these topics is broad, as proved by the several articles published in journals and conference proceedings.

Finally, reducing as much as possible the most expensive elements, like retardation plates or optical fiber launcher, can further decrease the cost of the optical set-up.

At present some portable speckle interferometers or part of these are available on the market, like the Dantec Dynamics interferometers for strain and vibration measurement [18], or NDT applications. Moreover technological centers specialized in optical techniques able to provide their metrological expertise can be easily found on the web, such as spin-offs or technology transfer centers.

Using commercial devices implies the advantages of not being involved in the issues of the correct implementation of the measurement equipment (i.e. alignment, calibration, optimization), and, above all, the users do not need an expertise on optical techniques. On the other hand using a "plug-and-play" interferometer, apart from the high initial cost, does not allow much flexibility, thus many adjustments cannot be performed because usually all the optical components of these devices are sealed into a closed case. Furthermore the software for managing the equipment, usually supplied by the seller with the hardware, provides only heavily processed output data; hence the image processing and the treatment of experimental data, which represent in speckle interferometry a critical stage of the measurement operations, cannot usually be controlled in detail.

The paper presents a low-cost portable interferometer working on the principles of speckle interferometry. The device is equipped with three laser diodes and a non-commercial piezoelectric actuator driven by a control electronics designed and realized on purpose. All the operations are controlled by a personal computer running in LabVIEW environment and interfaced with the control electronics by a USB port, and with the CCD camera by a Fire-Wire port. The interferometer allows measuring three displacement components by which the whole 3D deformation field can be retrieved.

2. The experimental equipment

The experimental equipment is formed by two parts: the interferometer and the control electronics interfaced with a laptop.

The interferometer is a compact and lightweight device based on Michelson design; a picture of the whole assembly is reported in Fig. 1. Three single mode laser diodes Hitachi model HL6512MG with an optical output power of 50 mW at 660 nm are used for illuminating the object along three different directions. The diodes are mounted in the assembly formed by the collimation tube (Thorlabs, model LT220P-B) and the strain relief/electrostatic discharge protection (Thorlabs, model SR9C).

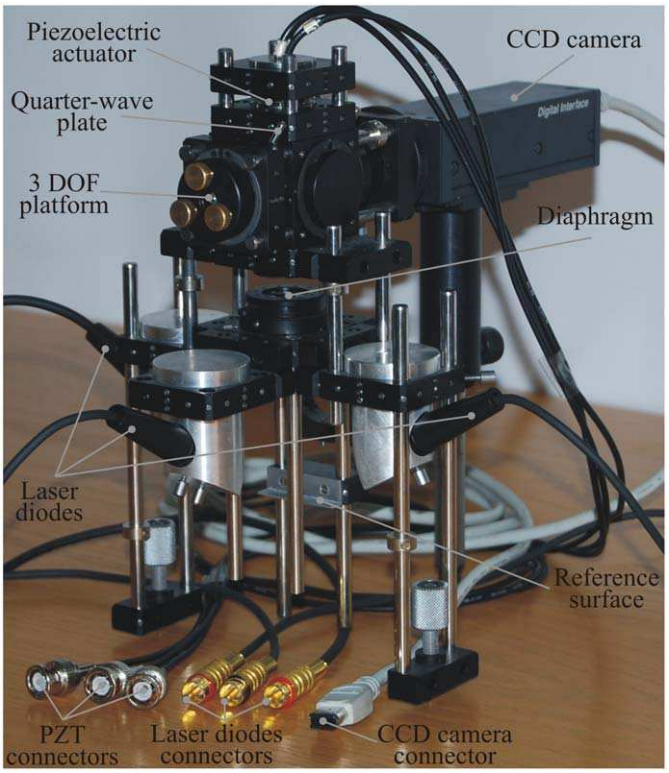

Fig. 1. The whole assembly of the speckle interferometer.

The interferograms are acquired by a Sony CCD camera model XCD-X710 with a sensor of 1024×768 pixels (pixel pitch $4.65 \times 4.65\,\mu m^2$). The camera is interfaced with a laptop by the IEEE-1394 Fire-Wire port and it can operate either in interlaced or in progressive mode. The observation direction is vertical, according to the picture reported in Fig. 1.

The piezoelectric actuator for applying phase-shifting procedure is a non-commercial device designed, realized and calibrated on purpose by the authors [14]. It is obtained by mounting three PZT ceramics Phisik Instrumente model PL033.30 into an elastic stainless steel case. The electro-mechanical solution adopted for realizing the actuator allows obtaining a highly rectilinear stroke of about 1.7 μm.

The imaging is obtained by two achromatic doublets, mounted in the opposite way with respect to the propagation direction of the light. In the experiments carried out in the present paper the two achromatic doublets used are LINOS model G322322000 (focal length 60 mm, lens diameter 22.4 mm) and model G322326000 (focal length 140 mm, lens diameter 22.4 mm). By mounting opposite each other the sides from/to which the parallel rays propagate, the image and the object planes are located at distances equal to the focal length from the respective doublet. In this way the magnification ratio, equal to ratio between the focal lengths of the doublets, can be varied discontinuously by substituting the doublet in front of the object plane with another one of different focal length, and without modifying the distance between the sensor of the CCD camera and its respective doublet.

Fig. 2 reports a section of the Michelson interferometer drawn from the 3D model used for designing the device. The two beams are obtained by a non-polarizing broadband cube beam-splitter, located between the achromatic doublets and thus operating on parallel rays. The object beam is sent to the CCD sensor by a mirror driven by the PZT actuator, while the reference beam is sent to the sensor by a second mirror mounted on a three

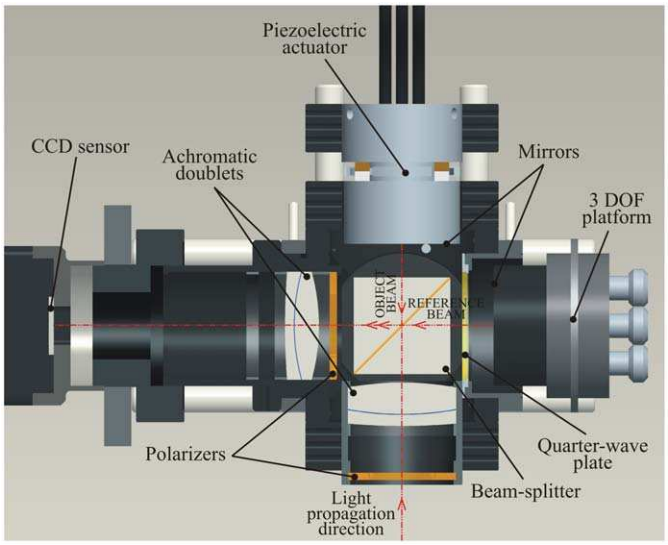

Fig. 2. 3D model of the Michelson interferometric layout.

degrees-of-freedom platform (recognizable by the adjustment screws visible in Figs. 1 and 2), necessary for the correct alignment with the piezo-actuated mirror.

The intensities of the reference and object beam, and thus their ratio, are adjusted by two rotating plates: a quarter-wave plate placed along the arm of the non-actuated mirror, and a polarizing plate placed between the beam-splitter and the doublet in front of the CCD camera. A further polarizer is placed at the entrance of the Michelson interferometer, in front of the first doublet. The use of this polarizer is not strictly necessary if the laser is polarized and the observed surface does not depolarize the light, but these two conditions are not necessarily contemporary fulfilled.

Apart from the first polarizer, all the optical elements are crossed by parallel rays, this fact implies good working conditions, minimizing the effects of aberrations.

The laser diodes and an iris diaphragm (for controlling the speckle dimension) are fixed on a module that can slide along four rods, in this way it is possible to illuminate the investigated area at different distance from the first doublet, and without modifying the angle of the illumination directions.

All these parts of the interferometer are assembled by using Linos Gmbh components (Microbench series system): modular mechanical elements in anodized aluminum that allow realizing stiff and high precision optical setups. The whole equipment is contained in a volume of about $200 \times 300 \times 300\,\mathrm{mm}^3$, the weight is about 2 kg (camera included). The position of the device is defined by three extendable legs, two of which can be finely adjusted by micrometers.

By the optical layout described above, the reference beam is obtained by imposing a slight misalignment of the mirror fixed to the three DOF platform. In this way the interference is obtained between the light scattered by two close surfaces placed not far from the observation axis. Therefore the interferometer can actually work as a shearometer, if the interfering points belong to the same surface, and it will measure the difference of displacement components. Otherwise, if a still surface is placed near the investigated surface, the interferometer is sensitive to the "absolute" displacement components.

The control electronics, assembled into a 19-in rack module, provides 9 output ports. In particular the first 4 ports (BNC connectors) provide the supply voltage for the piezoelectric low-voltage ceramics, this voltage can be varied in the range 0–100 V with the resolution given by a 16 bit digital-to-analog converter. The second 4 ports (RCA connectors) provide the supply voltage for the laser diodes, in this case a 12 bit DAC is used for supplying a voltage in the range 0–3 V. Under each of these 4 ports a system formed by two plugs allows placing a resistor for controlling the current of the laser diodes. A final port (DIN connector) is available for driving two DC motors, but in the present work they will not be mentioned any longer.

In the rear panel of the control electronics a serial port (RS-232) is present and it allows sending commands to set the voltage of each port via software by the laptop; the cable which connects the laptop to the control electronics adapts the USB port of the laptop to the serial port RS-232 of the control electronics. The commands to the port can be sent by the standard routines for input–output operations available in the conventional software environment normally used for instrumentation control, i.e. National Instruments LabVIEW or MatWorks Matlab-Simulink.

2.1. Illumination adjustment

In order to optimize the modulation of the interfering light fields two polarizing plates and a quarter-wave plate have been employed in the interferometer [19]. In particular Fig. 3 explains how the plates allow equalizing the two interfering beams. The object beam – Fig. 3a – hits only the two polarizers, thus the amplitude of outgoing object field u_{oo} can be evaluated as follows:

$$u_{oo} = u_{oi} \cos \beta, \tag{1}$$

with u_{oi} object field outgoing from the first polarizing plate and β angle between the two axes of polarization (P_i and P_o).

On the other hand the reference beam – Fig. 3b – hits the two polarizing plates and the quarter-wave plate. When polarized light gets through the quarter-wave plate two times, this acts like a half-wave plate and rotates the polarization axis symmetrically with respect to the fast axis of the plate. Hence the amplitude of outgoing reference field u_{ro} can be evaluated as follows:

$$u_{ro} = u_{ri} \cos (\beta - 2\alpha), \tag{2}$$

with u_{ri} reference field outgoing from the first polarizer, u'_{ri} reference field outgoing from the quarter-wave plate and α angle between the axis of ingoing polarizer (P_i) and the fast axis of the retardation plate (F).

If Eq. (1) is set equal to Eq. (2) the solution of the equation yields the pairs (α, β) which satisfy the optimal condition of interference [20]. Fig. 4 provides a family of curves for evaluating the aforementioned pairs; these curves are parameterized by the ratio between the intensities of the ingoing object and reference beams, obtained by squaring the ratio of the corresponding field amplitude, $(u_{oi}/u_{ri})^2$. The graph shows that for each intensity ratio two pairs exist which satisfy the condition of equal intensity for the two interfering beams.

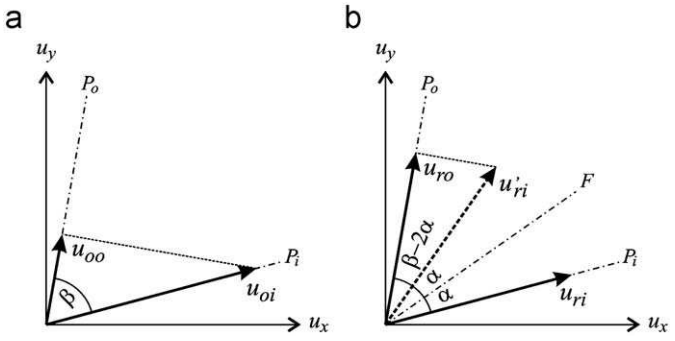

Fig. 3. Amplitude of the light fields: (a) object beam; (b) reference beam.

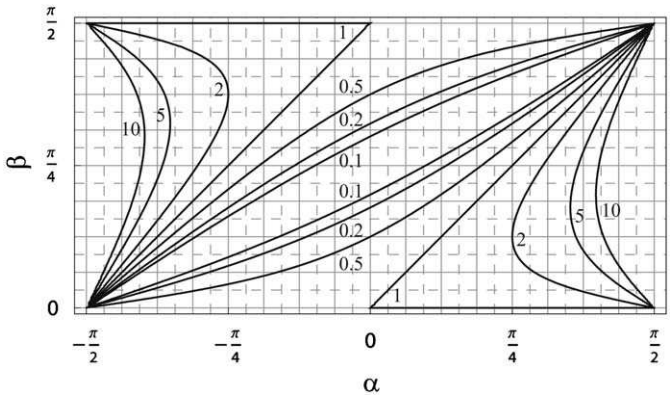

Fig. 4. Values of α and β for obtaining equal intensity (object and reference) beams at different ingoing intensity ratios $(u_{oi}/u_{ri})^2$.

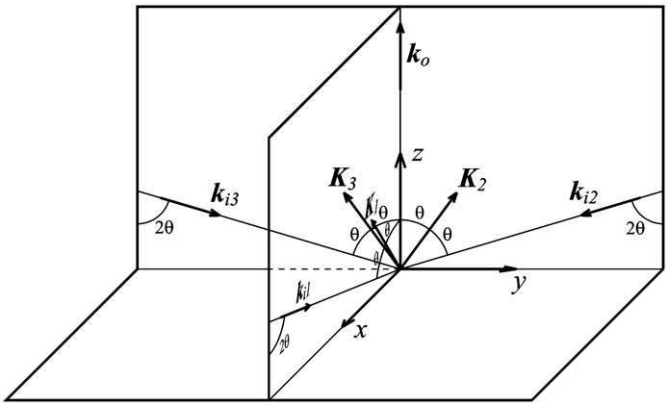

Fig. 5. Geometry of the illumination and observation directions adopted for measuring three components of displacement.

The equalization of the light intensity of the two interfering beams is necessary since this condition is not automatically satisfied in the optical layout. In fact the reference surface is fixed on the interferometer, and its scattering properties in general are different from those of the investigated surface. Furthermore each diode illuminates both reference and investigated surfaces, consequently the uniformity of the illumination is hardly achievable.

3. Measurement of 3D deformation fields

Measurement of 3D deformation fields requires the evaluation at each point of three displacement components. Speckle interferometry techniques allow measuring a single displacement component by means of an "absolute" interferometer working with a single illumination and observation direction [21]; actually the same effect can be attained with a shearometer working with a fixed reference surface. Thus by three non-coincident illumination directions the displacement can be fully resolved in all its components.

If at a generic point the illumination and observation directions are known and identified by the unit vectors $\boldsymbol{k}_i$ and $\boldsymbol{k}_o$, respectively, the sensitivity vector $\boldsymbol{K}$ can be evaluated by the well-known formula in holographic interferometry [22]:

$$\boldsymbol{K} = \boldsymbol{k}_o - \boldsymbol{k}_i. \tag{3}$$

The phase variation ϕ due to the generic 3D displacement $\boldsymbol{d} = \{u, v, w\}$ can be evaluated by the following equation:

$$\phi = \frac{2\pi}{\lambda}\boldsymbol{K}\cdot\boldsymbol{d} = \frac{2\pi}{\lambda}(K_x u + K_y v + K_z w), \tag{4}$$

where λ is the wavelength of the light source used in the experiments. Hence if three linearly independent sensitivity vectors are available, as shown in Fig. 5 which represents schematically the operating conditions of the present interferometer, the vector $\boldsymbol{d}$ can be fully resolved on the whole investigated area. If the three phase measurements $\{\phi_1, \phi_2, \phi_3\}$ are carried out at each point the 3D displacement can be resolved by the following expression, written in matrix form:

$$\begin{Bmatrix}\phi_1\\ \phi_2\\ \phi_3\end{Bmatrix} = \frac{2\pi}{\lambda}\begin{bmatrix}K_{1x} & K_{1y} & K_{1z}\\ K_{2x} & K_{2y} & K_{2z}\\ K_{3x} & K_{3y} & K_{3z}\end{bmatrix}\begin{Bmatrix}u\\ v\\ w\end{Bmatrix}. \tag{5}$$

The unique condition for solving the linear system of Eq. (5) is that the determinant of the matrix is different from zero, i.e. the three illumination directions must be linearly independent. In case of the present interferometer the observation direction is orthogonal to the investigated surface, while the angle θ indicated in Fig. 5 is chosen equal to 30° for all the three illumination directions and the sensitivity vectors lie in the planes *xz* and *yz*.

By applying Eqs. (3) and (5) in the aforementioned operating conditions, the following expression for the displacement components is obtained:

$$\begin{Bmatrix}u\\ v\\ w\end{Bmatrix} = \frac{\lambda}{2\pi}\begin{bmatrix}\frac{2\sqrt{3}}{3} & -\frac{\sqrt{3}}{3} & -\frac{\sqrt{3}}{3}\\ 0 & \frac{\sqrt{3}}{3} & -\frac{\sqrt{3}}{3}\\ 0 & \frac{1}{3} & \frac{1}{3}\end{bmatrix}\begin{Bmatrix}\phi_1\\ \phi_2\\ \phi_3\end{Bmatrix}. \tag{6}$$

In Eqs. (5) and (6) the same wavelength was assumed for all the displacement components. It must be noticed that this is an approximation usually acceptable when using laser diodes, in spite of the wavelength sensitivity of this type of light source to some operating parameters, like supply voltage or environmental temperature.

If the illumination is not obtained by a collimated beam, its divergence must be taken into account as the components of the sensitivity vectors become functions of the spatial coordinates. In this case the matrices of Eq. (5) or Eq. (6) must be evaluated at each point by taking into account the actual geometry of the setup, i.e. the location of the light source with respect to the orientation and position of the investigated surface. This effect can be neglected if the maximum dimension of the observed area is negligible if compared with the distance between the light source and the observed area.

3.1. Sensitivity correction

If the geometry of the setup does not allow neglecting the variation of the sensitivity vector along the observed area, this effect can be easily evaluated by straightforward mathematical expressions. In particular, according to the geometry reported in Fig. 6, if a spherical wavefront is located on the *xz* plane at an horizontal distance *L* from the origin of the reference system, and the light propagation occurs along a direction forming at the origin of the reference system an angle of 60° with respect to the vertical direction (as it happens in the interferometer presented in the paper), the sensitivity vector, after some mathematical

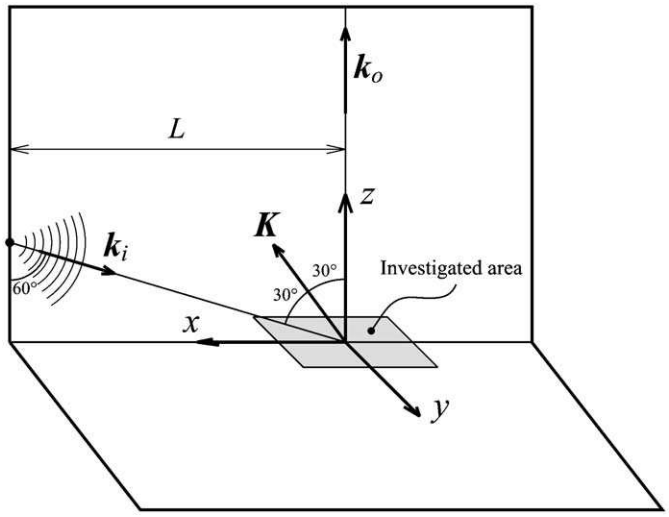

Fig. 6. Geometry for evaluating the variation of the components of the sensitivity vectors.

manipulations of Eq. (3), assumes the following expression:

$$\boldsymbol{K} = \left\{\frac{L-x}{A}, -\frac{y}{A}, \frac{L}{A\sqrt{3}} + 1\right\} \text{ with } A = \sqrt{(x-L)^2 + y^2 + L^2/3}, \qquad (7)$$

where the coefficient A represents the distance between the location of the spherical wavefront and the origin on the reference system. In this expression the observation direction is assumed constant, but also this assumption could be easily removed. If this effect is taken into account, as above mentioned, the matrix of Eq. (6) must be evaluated point by point, otherwise the evaluation of the elements of matrix can be carried out by means of Eq. (7), evaluated at the origin of the coordinate system. In this last operating condition the values for the components of sensitivity vectors are the following:

$$K_{1x} = K_{2y} = -K_{3y} = \frac{\sqrt{3}}{2} = 0.866$$

$$K_{1y} = K_{2x} = K_{3x} = 0$$

$$K_{1z} = K_{2z} = K_{3z} = \frac{3}{2} = 1.5, \qquad (8)$$

which can be assumed as reference values for evaluating their variation along the observed area. It is worthwhile mentioning

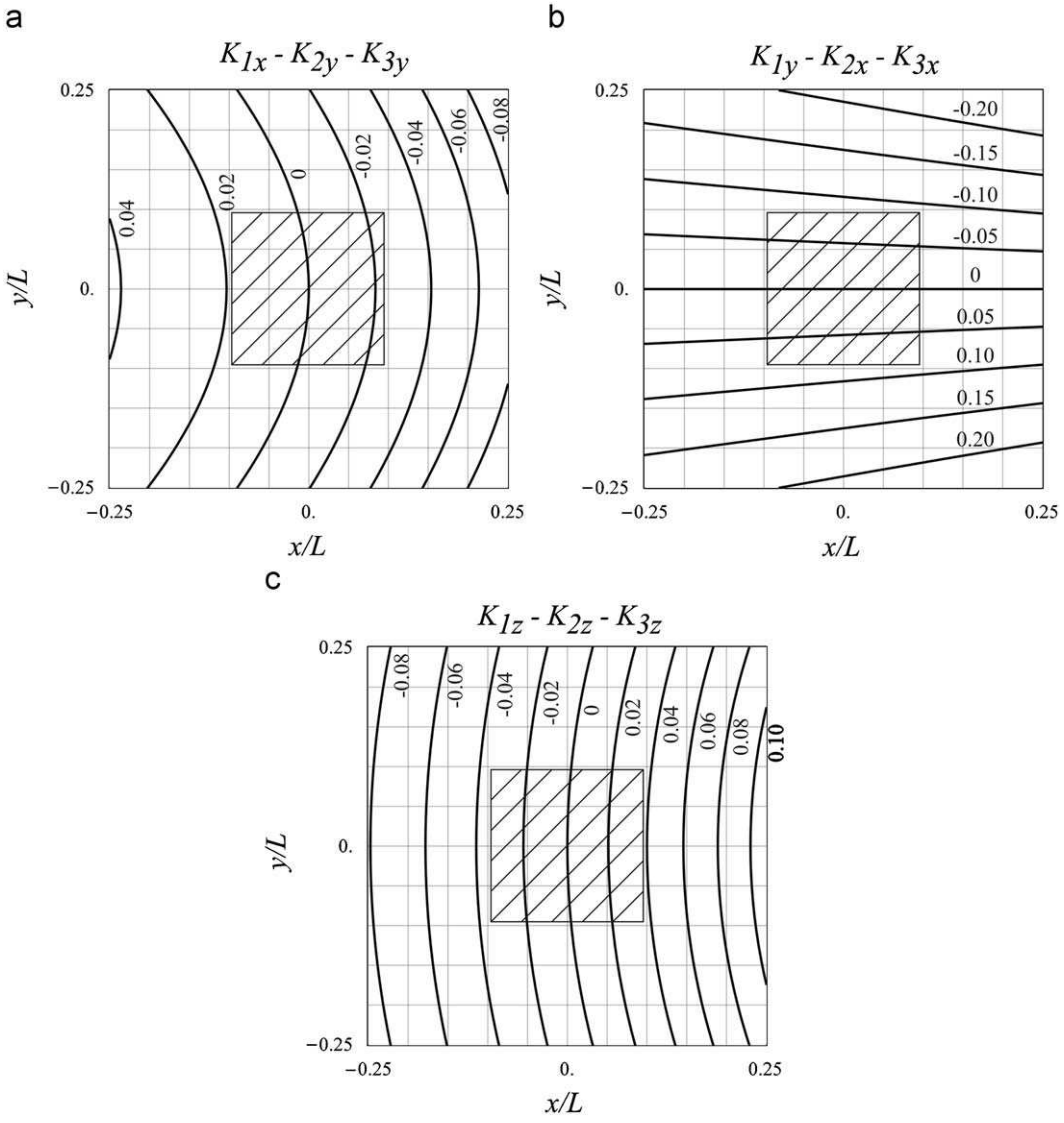

Fig. 7. Variation of the components of the sensitivity vectors with respect to non-dimensional coordinates x/L and y/L: (a) non-zero in-plane sensitivity components (K_{1x}, K_{2y}, K_{3y}); (b) zero in-plane sensitivity components (K_{1y}, K_{2x}, K_{3x}); (c) out-of-plane sensitivity components (K_{1z}, K_{2z}, K_{3z}).

that the maximum absolute value for a component of a sensitivity vector in interferometry is 2.

Fig. 7 reports the contour plots in the plane xy that represent the loci of constant error of the sensitivity vectors. Due to the symmetry of the illumination geometry, by three plots it is possible to evaluate the error for all the nine components of the sensitivity vectors, provided that the x and y coordinated are properly exchanged or reversed. In figure the spatial coordinates x and y are evaluated as fractions of the length L. In the case of the actual geometry of the interferometer the length L is about 55 mm and the investigated area about $8 \times 6\,\text{mm}^2$, hence the maximum range assumed for the ratios x/L and y/L is about 0.15. In figure the area corresponding to a maximum range for the ratios x/L and y/L of 0.2 is emphasized; within this area, which overestimates the real working area of the interferometer, the maximum variations observed do not exceed 0.02 for the components K_{1x}, K_{2y} and K_{3y}, 0.1 for the components K_{1y}, K_{2x} and K_{3x}, and 0.04 for the components K_{1z}, K_{2z} and K_{3z}. The resulting error on the measured displacement cannot be evaluated a priori because it depends on the entities and ratios between the single components of displacement.

3.2. Strain evaluation

When the 3D displacement field is measured by speckle interferometry, this is usually superimposed to a rigid body motion of the whole investigated area, which is normally an unwanted effect for several reasons. First, it is not easy to identify the absolute fringe order especially for a 3D problem, which requires the knowledge of three absolute fringe orders; sometimes it is possible to know the displacements of some points of the observed area, but it is not a common working condition, in particular when the measurements are carried out on small regions. Moreover, when the mechanical behavior of a material is investigated rigid body motions could make difficult identifying the desired information, whereas the strain components, computable by differentiating the displacement vector with respect to the spatial coordinates, would be unaffected by this drawback.

If the spatial distribution of the vector $\boldsymbol{d}$ is evaluated in the xy plane, the strain components can be computed according to the well-known equations of the theory of elasticity:

$$\varepsilon_x = \frac{\partial u}{\partial x} \varepsilon_y = \frac{\partial v}{\partial y} \gamma_{xy} = \frac{\partial u}{\partial y} + \frac{\partial v}{\partial x}$$

$$\varepsilon_z = \frac{\partial w}{\partial z} \gamma_{yz} = \frac{\partial v}{\partial z} + \frac{\partial w}{\partial y} \gamma_{zx} = \frac{\partial w}{\partial x} + \frac{\partial u}{\partial z}. \tag{9}$$

Actually only the first row of Eq. (9) can be evaluated, because the variation along the z coordinate cannot be retrieved by a speckle technique. Nevertheless, due to the plain stress conditions occurring on a free load surface [23], the components γ_{yz} and γ_{zx} are zero everywhere, while ε_z can be evaluated by the following equation:

$$\varepsilon_z = -\frac{v}{1-v}(\varepsilon_x + \varepsilon_y), \tag{10}$$

where v is the Poisson's ratio of the material.

Two final remarks must be made about the evaluation of strain components. The first one concerns with the smoothness of the measured quantities. The differentiation amplifies the noise usually high when speckle interferometry is applied for measuring deformations, hence filtering [24] or fitting [25] the experimental data is mandatory for obtaining consistent results. Secondly, if the investigated area is not planar the strain evaluation could be difficult, because the shape of the surface must be taken into account in the analytical formulation.

Therefore the post-processing of the experimental data in speckle interferometry is an important phase of the overall measurement process: a normal practice usually strictly dependent on the specific problem which must be approached. For this reason a general-purpose software for analyzing experimental data hardly suites all the needs of users of interferometric techniques. Consequently who tries his hand at speckle techniques should also plan proper post-processing procedures of the experimental data, if accurate and "actual" full-field measurements are required.

4. Experimental results

The capability of the interferometer to measure the 3D deformations was tested by imposing a 3D rigid body motion to a specimen moved by a three degrees-of-freedom PZT actuator. According to Fig. 8, by imposing two rotations (α_y and α_z around y- and z-axis, respectively), the three components of displacement can be evaluated by the following relation:

$$\boldsymbol{d} = \begin{Bmatrix} u \\ v \\ w \end{Bmatrix} = \begin{Bmatrix} -\alpha_z y \\ \alpha_z x \\ \alpha_y x \end{Bmatrix} \tag{11}$$

A first set of tests was carried out increasing by steps the entity of the rigid body motion, taking the initial values of the rotations equal to $\alpha_y = 0.125$ mrad and $\alpha_z = 0.145$ mrad; the subsequent values are equal to 2, 3 and 4 times the initial ones.

The axes of revolution of the specimen were chosen coincident with the reference axes, although it was not possible to locate them very accurately, because the specimen was positioned manually and the observed area is particularly small ($5.4 \times 5.4\,\text{mm}^2$). Anyway in order to compare among them all the experimental data acquired in the different operating conditions, the processing was carried out by assuming in the unwrapping procedure the zero of all the displacement components at the origin of the reference system.

An example of four full sets of experimental data is reported in Fig. 9. Each row represents the phase maps of the three displacement components for the rigid body motion due to the rotations given by the label placed on the left side of the row. The maps were obtained by applying the 5-step (equispaced) phase-shifting procedure.

The experimental data were fitted according to the method proposed in Ref. [25]. After the unwrapping, the phase variation of each map (a matrix of 500×500 elements) was described analytically by 25 (5×5) parabolic blending function according to the B-spline formulation. Actually, due to the particular deformation measured by the interferometer (a rigid body motion

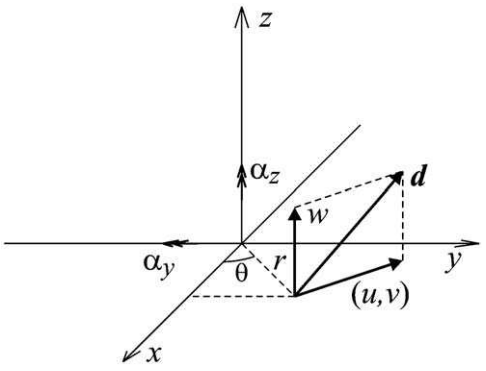

Fig. 8. 3D rigid body motion imposed to the specimen by the PZT actuator.

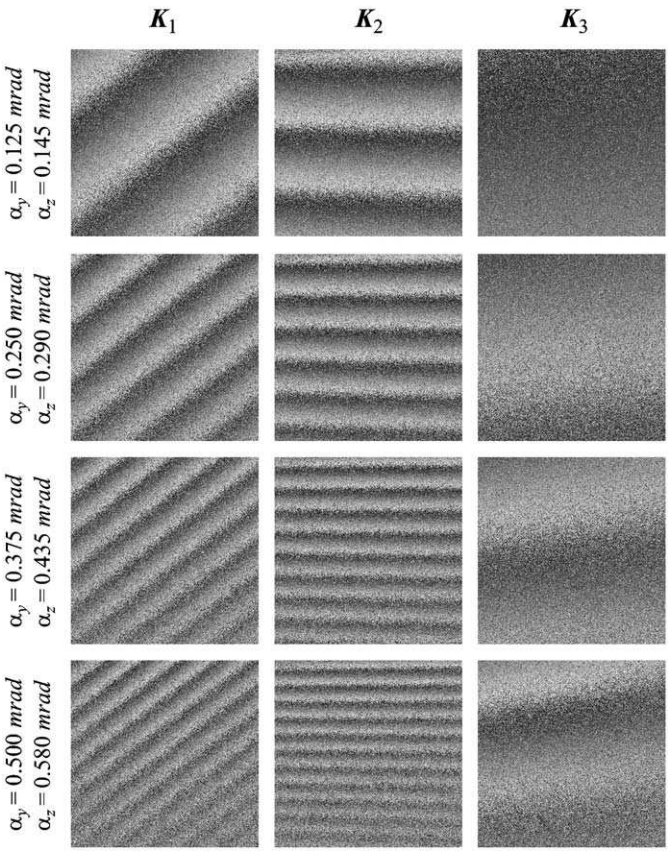

Fig. 9. Full sets of experimental data for four different levels of rigid body motion.

implies a linear variation of the phase), a fitting by linear functions should have been more accurate and straightforward. In fact a linear fitting requires the evaluation of 3 parameters for each phase map rather than 25 and a linear model would match exactly the actual displacement field. The followed approach aims to evaluate the performance of the fitting procedure which is necessity to adopt when generic displacement field is measured by an experimental technique, and the analytical model which best fits the problem is not known a priori.

The displacement components retrieved by the whole procedure (image acquisition, phase-shifting, unwrapping and fitting) are reported in Fig. 10. For each deformation field the three displacement components were used for evaluating the modulus of the in-plane component (the first column of plots) and the out-of-plane component (the second column of plots). The contour fringes of the plots are displayed every 100 nm: in particular for the in-plane components the continuous contours are displayed every 500 nm, while for the out-of-plane components the continuous contours represent the zero displacement (i.e. the axis of revolution of the rotation α_y). The zero in-plane displacement occurs at a single point, at the center of the circular fringes, and it is not displayed in the figure.

For each deformation field three different tests were reported, in order to evaluate the repeatability of the whole measurement procedure. A high repeatability was observed up to the third level of deformation, while at the fourth level the procedure failed to give good results, in fact by observing the plots of the fourth row of Fig. 10 it is possible to notice that the contours in the lower part of the investigated area are not regular. Actually the failure of the measurement procedure is not a discontinuous phenomenon which occurs when the displacement exceeds a fixed value, but it is a progressive corruption of the experimental data due to the decorrelation of the speckle patterns [26]. Also by observing the phase maps of Fig. 9 it is possible to notice in the third and in the fourth row a blurring of the maps in the lower part of the investigated area.

In case of the deformation field adopted in the experimental tests, the asymmetry of the contour plots, particularly evident for the in-plane components, is due to the non-perfect symmetry of the displacement field with respect to the reference system fixed on the specimen by the optical system. In fact, if the axis of revolution of α_z is not perfectly coincident with the z-axis, the maximum in-plane displacement does not occur symmetrically at the four corners of the image, and the area characterized by high error starts appearing in the zone of the observed surface farthest form the effective axis of revolution.

Finally it must be pointed out that the decorrelation can be partially recovered, minimizing the errors on the region of interest, by exploiting all the three degrees-of-freedom of the PZT actuator. At the moment only the uniform translation of the actuator is used for applying phase-shifting procedure, but the application of a tilting implies a translation of the image on the CCD of the camera, and this allows recovering the image-plane decorrelation, which is the phenomenon that, in the actual operating condition, mainly affects the accuracy of the measurements.

4.1. Error sources

As it was emphasized in previous section the decorrelation of the speckle fields implies a gradual corruption of the phase information. This unwanted (but unavoidable) effect arises from the displacement field, consequently it is intrinsic to the speckle measurement technique and impossible to be completely removed, at most it can be contained.

Roughly it can be stated that the in-plane displacements imply an image-plane decorrelation, while the out-of-plane displacements induced by rotations simply a pupil-plane decorrelation [27]; the two types of displacement can thus be analyzed separately. In the particular case of the interferometric layout proposed in the present paper, we have observed that the image-plane decorrelation is much more troublesome than the pupil-plane decorrelation; apart from the fact that it normally implies a narrower range of measurement, a uniform in-plane rigid body motion introduces a widespread decorrelation without providing any useful information.

By means of the specimen used in the experiments the same displacement fields measured and reported in Figs. 9 and 10 were superimposed to a uniform in-plane rigid body motion. The new displacement components measured in these new operating conditions are reported in Fig. 11. In particular the plots of first two columns are relative to a uniform in-plane rigid body motion in the horizontal direction equal to 2 μm (20% of the pixel pitch), whereas for the plots of the last two columns the entity of the disturbance motion is 4 μm (40% of the pixel pitch). As shown by Fig. 11 an increasing entity of the disturbance implies a reduction of the maximum displacement which can be retrieved by the technique. Thus the measurement procedure works almost properly if no disturbance is present and a maximum in-plane displacement roughly equal to 2 μm (last row of Fig. 10). On the other hand for a disturbance equal to 2 μm the maximum retrievable in-plane displacement is about 1.7 μm (last row of Fig. 11), while for a disturbance of 4 μm the procedure fails for a maximum in-plane displacement of about 0.5 μm.

Another source of inaccuracy is the variation of the sensitivity vectors along the investigated area. As already mentioned in Section 3.1 this effect is normally neglected, but in the case of the

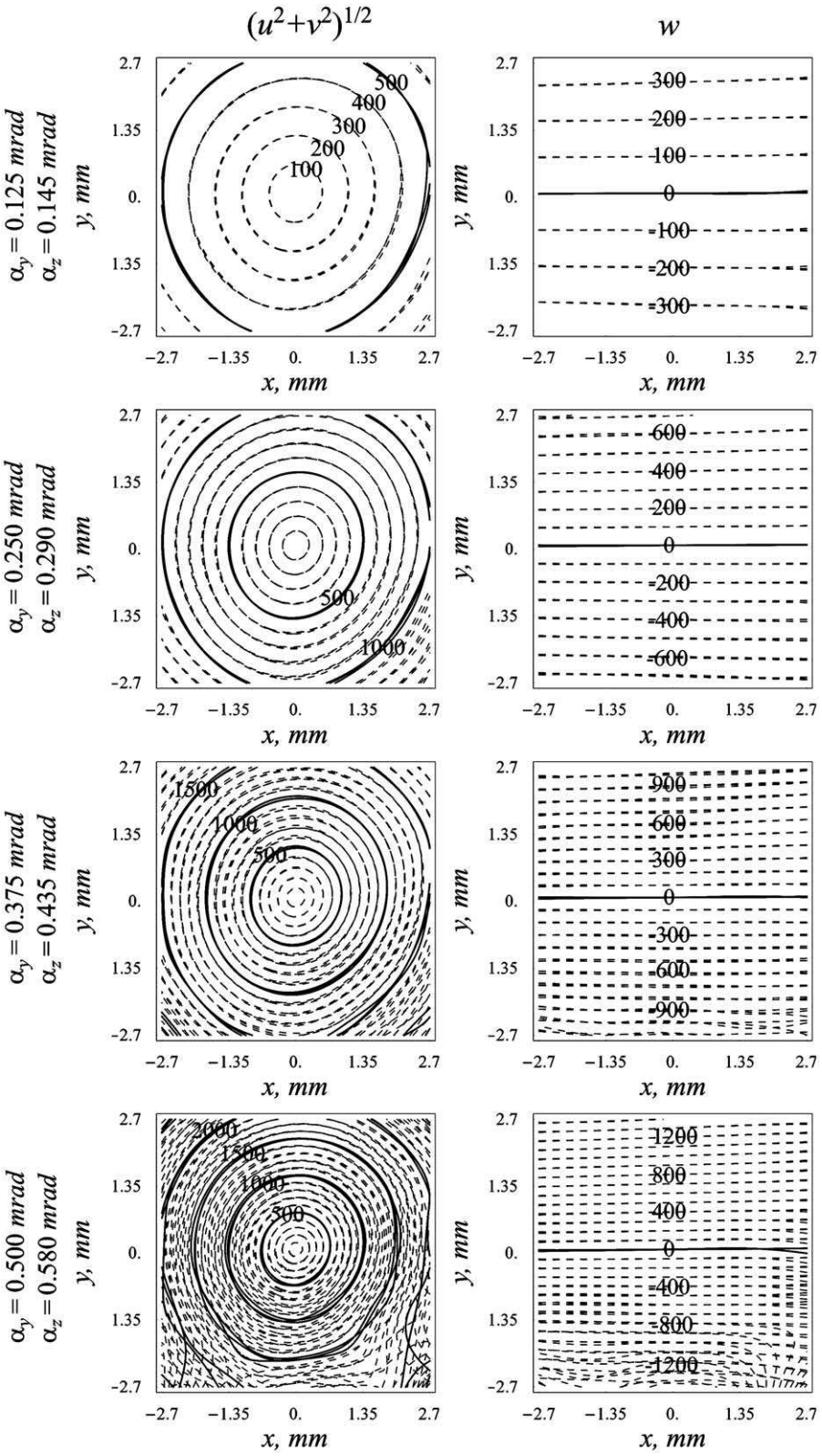

Fig. 10. Contour fringes of the fitted data at four different levels of deformation.

optical configuration adopted in the present work it is not exactly true. For the particular displacement field imposed to the specimen the contour plots should be concentric circumferences (for the modulus of the in-plane component) and straight lines (for the out-of-plane component). When the measurements are performed by considering the sensitivity vectors constant over the investigated area the aforementioned circumferences and straight lines are distorted. For instance Fig. 12 reports the contour plots obtained by neglecting this effect (dot-dashed line) and by taking into account this effect (continuous line)—the plots are obtained

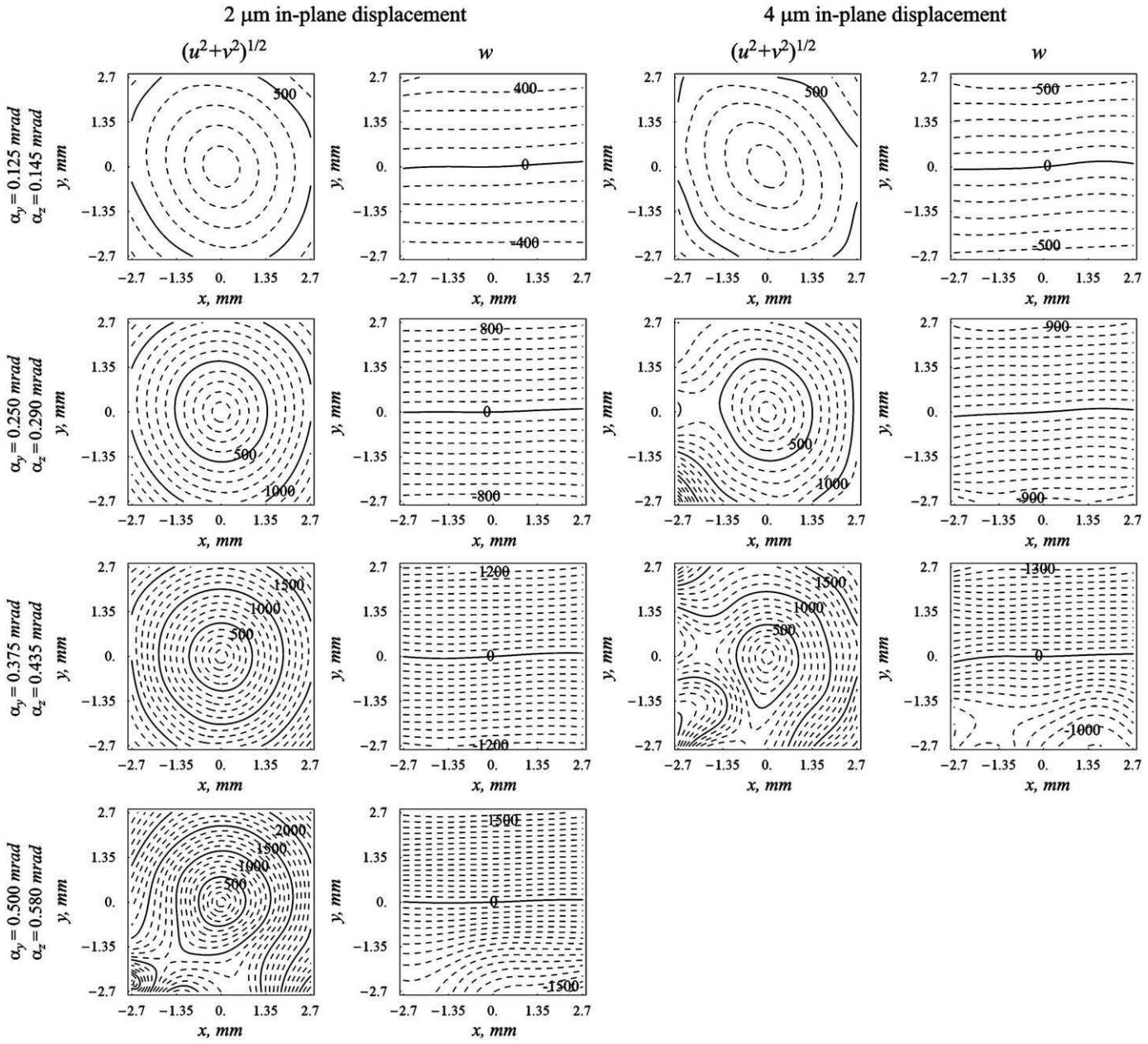

Fig. 11. Contour fringes of the fitted data at four different levels of deformation with 2 μm and 4 μm in-plane displacement.

by numerically simulating the displacement fields. In the first row of Fig. 12 the displacements are obtained by fixing the zero of each component at the origin of the axes, while the plots of the second row are obtained by displacing the zero of 1 mm in the vertical direction and of 4 mm in the horizontal direction. It is possible to notice that the entity of the distortion depends on the entity of the displacement, if the exact locations of the zero of each component are not known. The compensation of this type of inaccuracy can be carried out analytically, if the exact geometry of the optical set-up (illumination and observation point positions) is known, or experimentally, if a known displacement field is applied to the specimen.

5. Conclusions

The paper presents a speckle interferometer able to measure the three components of displacement occurring on small areas. The interferometer was designed and realized with the aim of obtaining a portable, low-cost and lightweight device mainly addressed for analyzing displacement field characterized by high gradients i.e. strain relief due to residual stress, deformations around notches and crack tips.

The costs of the device were reduced by using three laser diodes and a PZT actuator realized and calibrated by the authors; the control electronics for the lasers and the actuator was designed and realized on purpose by standard electronic components. Furthermore the optical components used in the interferometer were chosen with the aim of reducing as much as possible the total cost of the device. All the operations necessary for carrying out the experiments were controlled in LabVIEW environment running on a notebook.

The interferometer was tested by a specimen subjected to a 3D rigid body motion. The three displacement components were measured at different levels of deformation in order to evaluate the maximum measurable displacement. In particular the in-

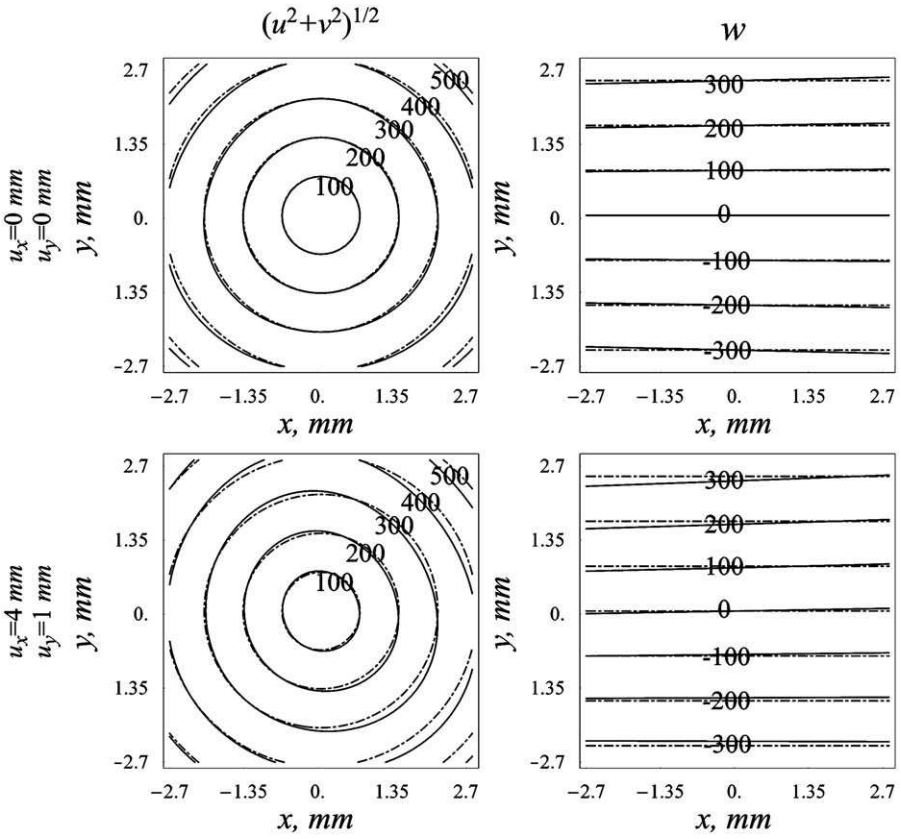

Fig. 12. Contour fringes obtained on numerical data with constant (dot-dashed curves) and variable (continuous curves) sensitivity vectors.

plane components came out very sensitive to the image-plane decorrelation, in fact the maximum in-plane displacement measurable by the interferometer drops significantly when the in-plane disturbance increases. On the other hand the out-of-plane component turned out less sensitive to this type of disturbance. In any case the measurement procedure has shown a high repeatability.

Some further improvements can be made to the experimental equipment. First of all a calibration of the interferometer will increase the accuracy of the measurement, in order to remove the error introduced by the variation of the sensitivity vectors due to the geometry of the optical set-up. Second, the image-plane decorrelation can be recovered by exploiting the two degrees of freedom of the PZT actuator not yet used. In fact at present, in order to apply a temporal phase-shifting procedure, the actuator is used only for obtaining a uniform translation of the mirror in the direction of the optical path. The use of the actuator for the recovery of the decorrelation requires a more advanced calibration procedure of the PZT device, not yet available. Finally the B & W CCD camera and the three red lasers can be substituted by a color CCD camera and a red, a green and a blue laser, in this way the measurement of the three components of displacement can be carried out simultaneously and a 3D real time application becomes conceivable.

References

[1] Archbold E, Burch JM, Ennos AE, Taylor PA. Visual observation of surface vibration of nodal patterns. Nature 1969;222:263–5.
[2] Leendertz JA. Interferometric displacement measurement on scattering surfaces utilizing speckle effect. J Phys E Sci Instrum 1970;3:214–18.
[3] Butters JN, Leendertz JA. Holographic and video techniques applied to engineering measurements. J Meas Control 1971;4:349–54.
[4] Leith EN, Upatnieks J. Reconstructed wavefronts and communication theory. J Opt Soc Am 1962;52:1123–8.
[5] Stetson KA, Molin NE. Measuring combination mode vibration patterns by hologram interferometry. J Phys E Sci Instrum 1969;2:609–12.
[6] Robinson DW, Reid GT, editors. Interferogram analysis. Bristol: IOP Publishing; 1993.
[7] Bhat GK. An electro-optic holographic technique for the measurement of the components of the strain tensor on three-dimensional object surfaces. Opt Lasers Eng 1997;26–1:43–58.
[8] Axelsson A, Marucci M. The use of holographic interferometry and electron speckle pattern interferometry for diffusion measurement in biochemical and pharmaceutical engineering applications. Opt Lasers Eng 2008;46–12: 865–76.
[9] Viotti MR, Albertazzi Jr AG, Kapp W. Experimental comparison between a portable DSPI device with diffractive optical element and a hole drilling strain gage combined system. Opt Lasers Eng 2008;46–11:835–41.
[10] Akhter N, Jung HC, Chang HS, Kim KS. Location of delamination in laminated composite plates by pulsed laser holography. Opt Lasers Eng 2009;47–5: 584–8.
[11] Dolinko AE, Kaufmann GH. Measurement of the local displacement field generated by a microindentation using digital speckle pattern interferometry and its application to investigate coating adhesion. Opt Lasers Eng 2009; 47–5:527–31.
[12] Maiman TH. Stimulated optical radiation in ruby. Nature 1960;187:493–4.
[13] Huntley JM, Ochoa NA. Convenient method for calibrating nonlinear phase modulators for use in phase-shifting interferometry. Opt Eng 1998;37–9: 2501–5.
[14] Bruno L, Poggialini A, Felice G. Design and calibration of a piezoelectric actuator for interferometric applications. Opt Lasers Eng 2007;45–12: 1148–56.
[15] Davila A, Landgrave JEA, Garnica G. In Situ calibration of a Michelson type, speckle-shearing interferometer: wobbling mirror effect. Opt Lasers Eng 2007;45–1:70–6.
[16] Patil A, Langoju R, Rastogi P. Phase shifting interferometry using a robust parameter estimation method. Opt Lasers Eng 2007;45–2:293–7.
[17] Bruno L, Maletta C. Real-time calibration of open-loop piezoelectric actuators for interferometric applications. Int J Mech Mater Des 2008;4–2: 97–103.
[18] http://www.dantecdynamics.com/.

[19] Shurcliff WA. Polarized light. Cambridge, MA: Harvard University Press; 1966.
[20] Lehmann M. Optimization of wavefield intensities in phase-shifting speckle interferometry. Opt Commun 1995;118:119–206.
[21] Bruno L, Poggialini A. Phase retrieval in speckle interferometry: a one-step approach. Proc Interferom Speckle Light Theory Appl Lausanne 2000: 461–72.
[22] Jones R, Wykes C. Holographic and speckle interferometry. Cambridge: Cambridge University Press; 1989.
[23] Timoshenko SP, Goodier JN. Theory of elasticity. New York: McGraw Hill; 1970.
[24] Federico A, Kaufmann GH. Denoising in digital speckle pattern interferometry using wave atoms. Opt Lett 2007;32–10:1232–4.
[25] Bruno L. Global approach for fitting 2D interferometric data. Opt Express 2007;15–8:4835–47.
[26] Sirohi RS, editor. Speckle metrology. New York: Marcel Dekker; 1993.
[27] Lehmann M. Decorrelation-induced phase errors in phase-shifting speckle interferometry. Appl Opt 1997;36–16:3657–67.